Publ. Astron. Soc. Japan 33, 449-464 (1981)

Neutral Hydrogen in M 31. I. The Distribution of H I Gas and Spiral Arms

Yoshiaki SOFUE and Tatsuji KATO

Department of Physics and Astrophysics, Nagoya University, Chikusa-ku, Nagoya 464

(Received 1980 November 8; revised 1981 January 24 and April 22)

Abstract

We propose a method to obtain the spatial distribution of the H I gas in a largely tilted (nearly edge-on) disk galaxy from velocity profiles of the H I line emission. Our method is applied to the data from the high-sensitivity, filled aperture survey of M 31 in the 21-cm H I line emission made with the 100-m radio telescope by Cram et al. (1980).

Resulting maps of the distribution of the surface density of the H I gas, $N_{\rm H\,I}$, in M 31 as seen face-on show a highly condensed "H I ring" of $N_{\rm H\,I}\geqq 4\times10^{20}\,{\rm cm}^{-2}$ at radii $R=8$ to 16 kpc, where approximately 54 percent of the total H I mass of M 31 is involved. The H I ring consists of a few dense arms and patches of peaks $N_{\rm H\,I}\geqq 6\times10^{20}\,{\rm cm}^{-2}$. A well-developed, *trailing* spiral arm is found at $R=20$–26 kpc in the south-west. The maps reveal further an extended H I disk of low surface density ($N_{\rm H\,I}\lesssim10^{20}\,{\rm cm}^{-2}$) which extends far out to $R=30$–35 kpc. The radial distribution of $N_{\rm H\,I}$ in the extended disk beyond $R=16$ kpc is plateau-like. The outermost part of the northern disk at $R\sim30$ kpc is associated with several faint, spur-like spiral arms. Some other remarkable features are discussed.

Key words: Galaxies; M 31; Neutral hydrogen; Spiral arms.

1. Introduction

A number of surveys of the neutral hydrogen (H I) in M 31 have been published Roberts 1966; Davies and Gottesman 1970; Gottesman and Davies 1970; Guibert 1973, 1974; Whitehurst and Roberts 1972; Shane 1975; Emerson 1974, 1976; Roberts and Whitehurst 1975; Cram et al. 1980; Unwin 1980a, b). M 31 has been studied extensively both at optical and at radio wavelengths. A detailed comparison between the various constituents has been given by Berkhuijsen (1977) and in the literature cited therein. The main features of the hydrogen distribution revealed by these studies are as follows: (a) H I emission is mainly concentrated on a ring-like structure of radius ~10 kpc; (b) The H I ring coincides with a ring of H II regions (Arp 1964; Baade and Arp 1964; Richter 1971; Pellet et al. 1978; Simien et al. 1978) and of OB associations (van den Bergh 1964). (c) The H I ring coincides with a radio continuum ring of nonthermal emission (Pooley 1969; Berkhuijsen 1977; Beck 1979; Beck et al. 1980). (d) Except for some H I-intensity peaks along the major axis, which coincide with some of Baade's (1958) arms, there has been no clear trace of H I spiral arms.

Recently Cram et al. (1980) have performed a complete, high-sensitivity, filled aperture survey of M 31 in the 21-cm H I line emission, using the Bonn 100-m telescope. In the present paper we analyse their data and study the H I gas distribution with regards to the gaseous spiral arms in M 31. We develop a method of velocity-to-space transformation (VST) with which a spatial distribution of the H I gas is determined from radial velocity data. Our method is similar to that proposed by Whitehurst et al. (1978), who intend to derive three-dimensional H I distribution in M 31. In a forthcoming paper we discuss dynamical and kinematical properties of the spiral structure of M 31 from a view point of the density wave theory (Sawa and Sofue 1981).

2. The Data

The data of the 21-cm line emission of M 31 we use here were obtained by Cram et al. (1980) with the 100-m Bonn telescope during 1974 and 1975. The half power beam width of the antenna was 8′.8. The receiver consisted of a cooled parametric amplifier with a total system-noise temperature of 60 K and a 384-channel autocorrelation spectrometer at a 2.75 km s^{-1} velocity interval. The effective velocity resolution is 5.5 km s^{-1} or 26 kHz. The rms noise in each velocity profile is typically 0.05 K. The mapped area covers $90' \times 300'$ centered on M 31 with a spacing of 4′.5, approximately half the beam width.

The results have been displayed in various formats by Cram et al. (1980) such as velocity profiles [$T_A(v)$: antenna temperature plotted against velocity] and iso-contour maps of $T_A(v, \lambda)$, $T_A(v, \beta)$ and $\int T_A(\lambda, \beta)dv$. The data are also presented in the form of velocity profiles on a magnetic tape written in a FORTRAN readable character format. We make use of the data on a magnetic tape, which includes 1260 velocity profiles each with 384 channels at 2.75 km s^{-1} interval, half of the velocity resolution.

A rectangular coordinate system (λ, β) is taken centered on R.A. $00^h40^m00^s$, Dec. 41°00′00″ (1950.0), the generally accepted optical center of M 31. The λ axis is the major axis of the galaxy, assumed at a position angle 38° from the north; and the β axis is the minor axis. Both λ and β are positive northword. Note that λ corresponds to the X, and β to the negative Y in the optical studies by Baade and Arp (1964) and Arp (1964). Our results are displayed in the (ξ, η) coordinate system which is introduced in the next section.

3. The VST (Velocity-to-Space Transformation) Method

Except for our Galaxy, maps of the spatial distribution of the H I gas in galaxies have been made from data on the integrated H I column density. Their angular resolutions have been limited by the antenna beam widths of the observations. In highly-tilted galaxies this circumstance has put a severe restriction on the study of the spatial distribution of hydrogen gas; even if the antenna beam is fairly sharp compared with the galaxy size, we still have much poor spatial resolution in the direction of the minor axis.

In case of M 31 the most reliable inclination angle lies between i=76° and 78° (Burke et al. 1964; Roberts 1966; Rubin and Ford 1970; Emerson 1976; Simien et al. 1978) (90° is edge on). We adopt i=77° throughout this paper,

which yields a major-to-minor axial ratio of 4.45 for a circular flat disk. The angular resolution of 9′ of the 100-m telescope in the 21-cm H I line observations corresponds to a spatial resolution of 1.8 kpc along the major axis (λ axis) at a distance of 690 kpc, and to 8.0 kpc along the minor axis (β axis). If we take into account the finite thickness of 100–200 pc for the disk, the widely accepted H I thickness of spiral galaxies, the spatial resolution along the minor axis reduces to 9 kpc. If the H I disk is thicker than this value as suggested by Whitehurst et al. (1978), the resolution should be much reduced. Such a low resolution is too poor to study spiral structures of the galaxy, because the antenna beam covers well more than two arms simultaneously.

We remember here how the positions of spiral arms in our Galaxy have been determined, despite the fact that we observe the Galaxy "edge-on." If we know the rotation curve of the Galaxy in circular motion, we are able to allocate the radial velocity to a certain depth on the line of sight in the galactic plane (e.g. Kerr and Westerhout 1965). We apply this method to the velocity data of M 31, with which we are able to transform from the observed velocity profiles to the corresponding spatial distribution. Whitehurst et al. (1978) have proposed a similar method to obtain a three-dimensional distribution of H I gas.

The present velocity-to-space transformation (VST) method consists of the following procedures: (a) to get the radial-velocity distribution (velocity field) over the entire disk of the galaxy, with which we are able to allocate an observed radial velocity at a fixed λ to the corresponding depth; (b) to get a radial-velocity profile at a fixed λ by adding the velocity profiles at various β so that the galaxy is observed by a "fan beam" elongated in the β direction but with the original resolution in the λ direction. This should be made separately for positive and negative β to avoid, as well as possible, the uncertainty in the allocation of the radial velocity to one of the two possible positions corresponding to the same velocity, although merging of the emission from the far and near sides cannot be avoided completely around the major axis (see section 3-iv); (c) to allocate all the velocity channels in each of the superposed profiles to the corresponding positions (depth) in the β direction by using the velocity field; (d) to transform the antenna temperature to the surface density, $N_{\mathrm{H\,I}}$, at the corresponding position.

(*1*) *The rotation curve*: Several authors have obtained the rotation curve of M 31 by using radial velocity data of H II regions and OB associations (Rubin and Ford 1970), the 21-cm H I line data (Roberts 1966; Roberts and Whitehurst 1975; Emerson 1976; Cram et al. 1980), and by combination of both the optical and radio data (Kormendy and Norman 1979). We here determine the rotation curve by use of the $T_{\mathrm{A}}(\lambda, v)$ diagram at $\beta=0$ obtained by Cram et al. (1980), which is reproduced in figure 1. On the diagram we trace local maxima so that small-scale fluctuations in velocity and intensity are smoothed out (thick line).

Figure 2 shows the rotation curves of M 31 thus obtained separately along the NE and SW halves of the major axis. The central velocity of $V_{\mathrm{c}}=-300\,\mathrm{km\,s^{-1}}$ (LSR) has been subtracted and the projection factor, $\sin i$ with $i=77°$, has been corrected. Figure 2 also compares our result with those obtained earliear as well as that for our Galaxy. We find a good agreement among them at $R\gtrsim 4$ kpc. Optical observations show more structures at $R\lesssim 4$ kpc, where our rotation curve cannot be trusted and results obtained in the central region of $R\lesssim 4$ kpc should not be considered seriously. We note that our rotation curves in figure 2 show a north-south asymmetry at $R=4$ to 15 kpc. The maximum rotation velocity $\Theta_{\mathrm{max}}=254$

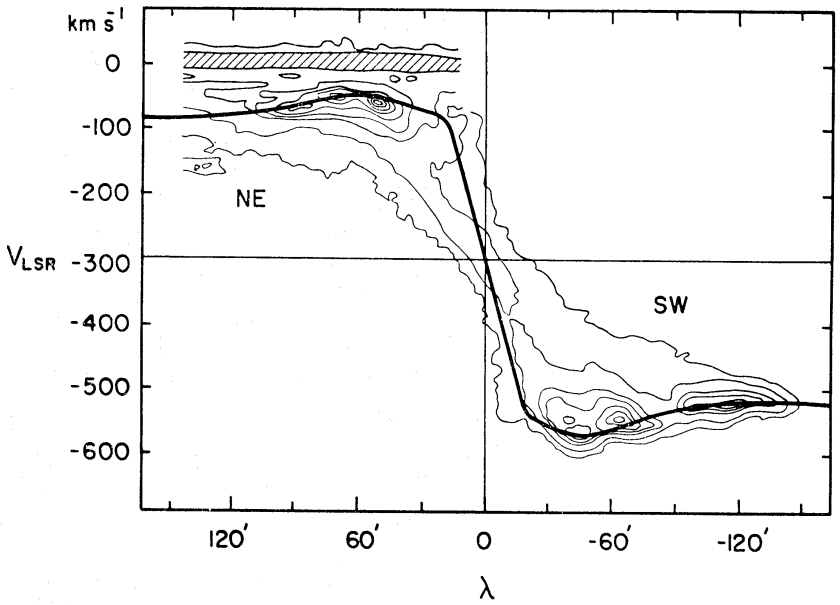

Fig. 1. Iso-T_A diagram in the (λ, v) coordinates along the major axis of M 31 ($\beta=0$). The solid line is used to derive the rotation curves in figure 2.

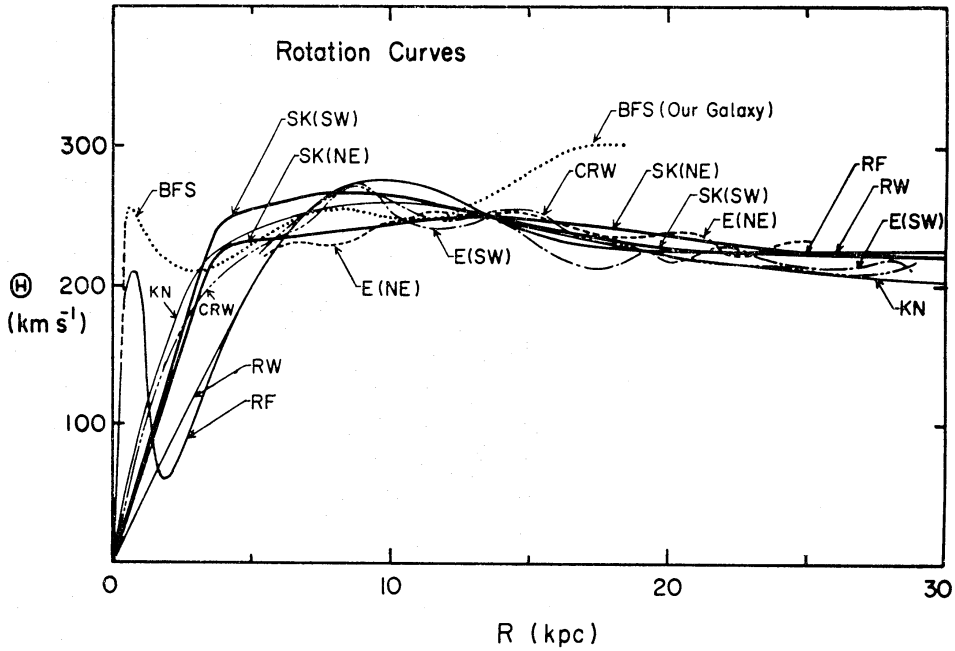

Fig. 2. The rotation curves along the major axis of M 31. For a comparison some rotation curves obtained by other authors for M 31 and the rotation curve of our Galaxy are drawn herewith. RW: Roberts and Whitehurst (1975); CRW: Cram et al. (1980); E: Emerson (1976); RF: Rubin and Ford (1970); KN: Kormendy and Norman (1979); BFS: Blitz et al. (1979) for our Galaxy; SK: present results.

km s^{-1} occurs at $R=13$ kpc for the NE rotation curve, and $\Theta_{max}=270$ km s^{-1} at $R=9$ kpc for the SW rotation curve. The rotation curves employed are approximately expressed by the following equation:

$$\Theta(R)=\Theta_\infty\left\{1+A\exp\left[-\left(\frac{R-R_{\max}}{B}\right)^2\right]\right\}, \quad (1)$$

where Θ_∞, $R_{\max}$, A, and B are constants. The parameters are given in table 1.

Table 1. Parameters for the rotation curve expressed by equation (1)* and the maximum velocity for M 31.

Parameter	NE	SW
A	0.13	0.20
B	7.0	6.0 kpc
$R_{\max}$	9.0	13.0 kpc
$\Theta_{\max}$.....	254	270 km s^{-1}
Θ_∞	225	225 km s^{-1}

* Equation (1) applies for $R\geq 3$ kpc. At $R<3$ kpc a solid rotation is assumed.

(2) *Velocity field*: To apply the VST method we need a radial velocity field over the entire disk of M 31. Making use of the rotation curves in figure 2 we construct an expected velocity field when the galaxy is observed at the inclination of $i=77°$. At $R\leqq 3$ kpc we assume a solid rotation. The radial velocity v is represented as

$$v(R,\theta)=V_c+V^*(R,\theta)\cos\theta\sin i \quad (2)$$

with

$$V^*(R,\theta)=[\Theta_N^2(R)\cos^2(\theta/2)+\Theta_S^2\sin^2(\theta/2)]^{1/2}, \quad (3)$$

where $\Theta_N(R)$ and $\Theta_S(R)$ are the rotation velocities along the NE and SW halves of the major axis, respectively. Here θ is the azimuthal position angle on the

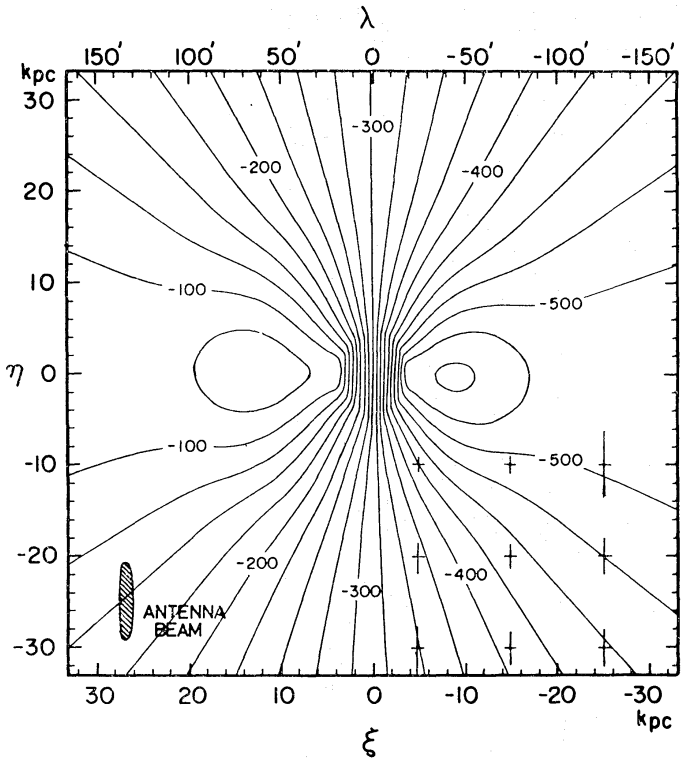

Fig. 3. The velocity field of M 31, or the distribution of radial velocity (LSR) over the disk in the (ξ,η) coordinate system. An asymmetry of the velocity field along the minor axis (Emerson 1976) is taken into account. Crosses represent the effective spatial resolution of the VST method at some points.

galaxian plane measured from the northern node, and V_c is the central radial velocity of M 31. Figure 3 shows the velocity field thus calculated as seen face on in the (ξ, η) coordinate system, where ξ and η are defined by $\xi=\lambda\times 690$ kpc, and $\eta=\beta\times 690/\cos i$ kpc. Note that the ξ and η are the X and negative Y, respectively, in earlier studies (e.g. Arp 1964).

(3) *The VST*: To allocate observed velocities to the corresponding depths in the β direction or η, we add the velocity profiles all over the β range at a fixed λ, separately for negative and positive β. Since the antenna beam of the 100-m telescope is well represented by a gaussian beam (Reich et al. 1976), the simple addition of all the profiles for $\beta=0'$ to $+36'$ and $\beta=0'$ to $-36'$ yields profiles when the galaxy is observed by an almost flat "fan" beam of $8'.8\times 36'$ (or 1.8 kpc$\times$32 kpc) centered on $\beta=\pm 18'$. Figure 4 is an example of the velocity profile thus obtained at $\lambda=-52'$.

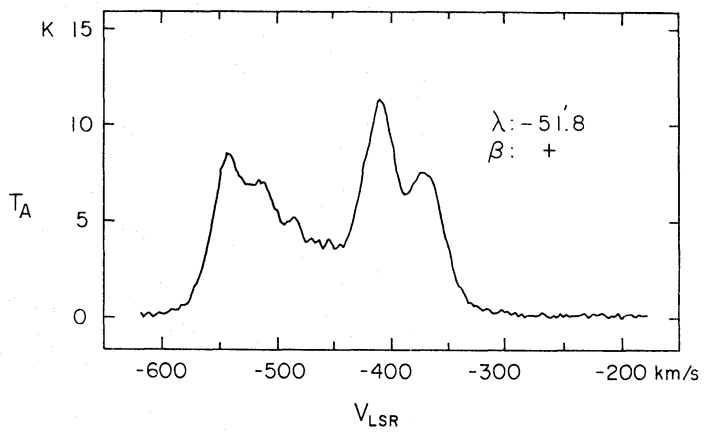

Fig. 4. Superposition of all the velocity profiles from $\beta=0'$ to $\beta=36'$ at $\lambda=-52'$. We transform this velocity profile into the spatial distribution of H I gas through the VST method.

We divide the disk of M 31 into meshes of $\Delta\xi\times\Delta\eta$ with $\Delta\xi=\Delta\eta=0.9$ kpc. Now for a fixed λ (or ξ), by using the velocity field in figure 3, we can allocate a velocity range from $v_1=v(\xi, \eta-\Delta\eta/2)$ to $v_2=v(\xi, \eta+\Delta\eta/2)$ for each cell centered on (ξ, η), separately for positive and negative η. In each cell we integrate the velocity profile from v_1 to v_2 and obtain an integrated antenna temperature $T_A^*(\xi, \eta)$ from the cell:

$$T_A^*(\xi, \eta)=\int_{v_1}^{v_2} T_A(v)dv \ . \qquad (4)$$

The surface column density of H I atoms, N_{HI}, as seen face on is proportional to T_A^*. The conversion factor to get N_{HI} from T_A^* is determined so that the integrated H I mass over the M 31 disk becomes equal to the total H I mass obtained by Cram et al. (1980): $M_{HI}=3.86\times 10^9 M_\odot$.

(4) *Accuracy and limitation of the VST*: The result of VST depends on the velocity field employed. The spatial resolution in the η-direction depends on the velocity resolution of the spectrometer. The resolution in the ξ-direction is, of course, the same as the antenna beam width, 8'.8 or 1.8 kpc. For a normal rotation curve and a uniform velocity resolution, the η resolution, $\delta\eta$, is given by

$$\delta\eta=\frac{\delta v}{|\partial v/\partial\eta|}\ , \tag{5}$$

with

$$\delta v=\left[\Delta v^2+\left(\frac{\partial v}{\partial\xi}\,\delta\xi\right)^2+v_t^{\,2}\right]^{1/2}\ , \tag{6}$$

where Δv is the velocity resolution of the spectrometer, $\delta\xi$ is the spatial resolution in the ξ-direction determined by the antenna beam, and v_t is the turbulent velocity of the H I gas in M 31. The larger is $|\partial v/\partial\eta|$ and the smaller is δv, the higher is the accuracy. The highest η-resolution is obtained in the middle region in each of the four sectors divided by the ξ and η axes. For example, at $(\xi,\eta)=$ (10 kpc, 10 kpc) we have $\delta\eta\cong 2$ kpc, which corresponds to an angular resolution of $2'$ in β. Low resolution occurs near the η-axis, and no resolution can be made in practice on the η-axis, where all the velocities are "degenerated" to the central velocity, V_c, yielding $\partial v/\partial\eta=0$. We have also low resolution near the ξ-axis where $|\partial v/\partial\eta|$ becomes small. Near the ξ-axis an uncertainty of the allocation of the velocity to η occurs because of the merging of emissions from positive and negative η regions (near and far sides of the major axis) in an antenna beam. This circumstance causes somewhat symmetric features in the H I distribution with respect to the ξ-axis at $|\eta|\lesssim 4$ kpc. Crosses in figure 3 indicate effective spatial resolution using the VST method at some typical points.

An advantage of the present method is that the result is not so much affected either by the uncertainty in the inclination of the galaxy or by the warping and corrugation of the disk. The estimated inclination of M 31 ranges from $i=74°$ to 79° (e.g. Arp 1964), which yields a wide range of possible η from $\eta=690\ \text{kpc}\times\beta/\cos 74°=0.728\beta'$ kpc to $690\times\beta/\cos 79°=1.05\beta'$ kpc for a flat and thin disk. At $\beta=20'$, for example, the possible η ranges from 14.6 to 21.0 kpc. Note that the velocity field constructed from the rotation curve (figure 3) varies only 2 percent in this range of inclination. The contamination of the foreground H I emission originating in our Galaxy reduces the accuracy in the region of $7\leqq\xi\leqq 20$ kpc and $|\eta|\lesssim 4$ kpc, where the highest radial velocity is obtained: $v\approx -50$ to $-70\ \text{km s}^{-1}$. Outside this region the effect of the foreground emission is negligible.

4. The Distribution of Neutral Hydrogen in M 31

Figures 5a–c show the distribution of the surface density of H I gas, $N_{\text{H I}}$, in M 31 as seen face on in the (ξ,η) coordinates. The rotation of the galaxy in the figure is counter-clockwise, and the positive side is the near side to us. Figure 6 emphasizes some "fine" structures by subtracting from the original map (figure 5) a smoothed distribution after a convolution with a gaussian beam with a half width of 6 kpc×6 kpc using the method described in Sofue and Reich (1979).

(*1*) *Main features*: Several main features obtained are summarized in figure 7 and are discussed below:

(a) "H I Ring:" A large-scale concentration of H I gas is found at radii $R=8$ to 15 kpc, forming the so called "H I ring." The weighted mean radius is 12 kpc. The outer edge of the ring, in particular in the SW side, is very steep. A typical column density of H I in this ring is $\sim 4\times 10^{20}\ \text{cm}^{-2}$, which yields a number density of H I atoms of $n_{\text{H I}}\sim 1.3\ \text{cm}^{-3}$ for a disk thickness of 100 pc.

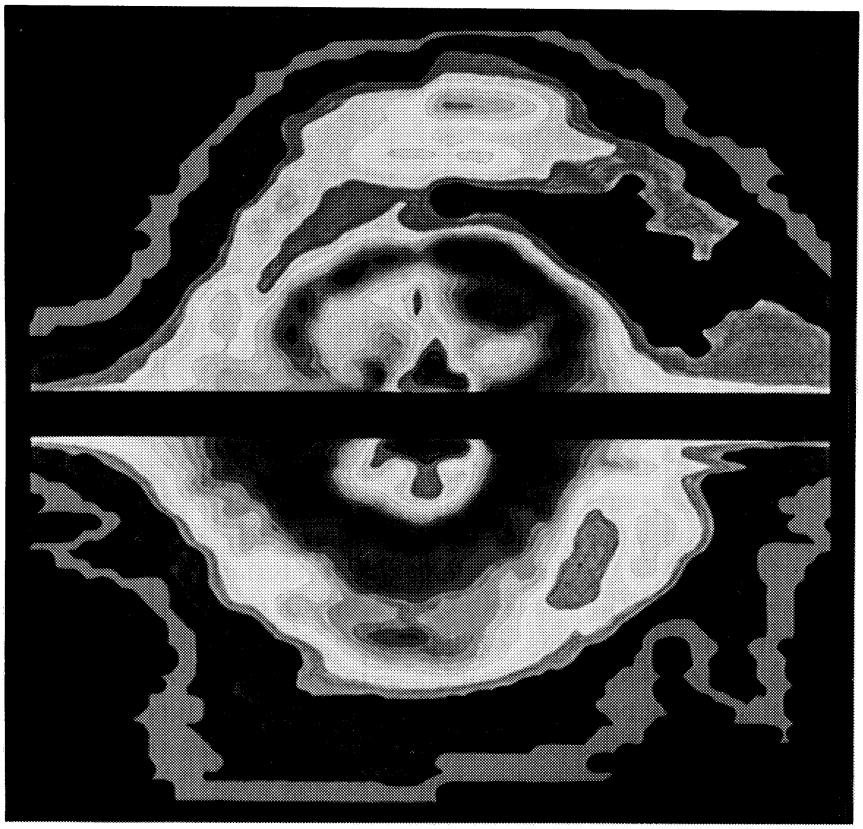

Fig. 5b. The same as figure 5c but displayed in color.

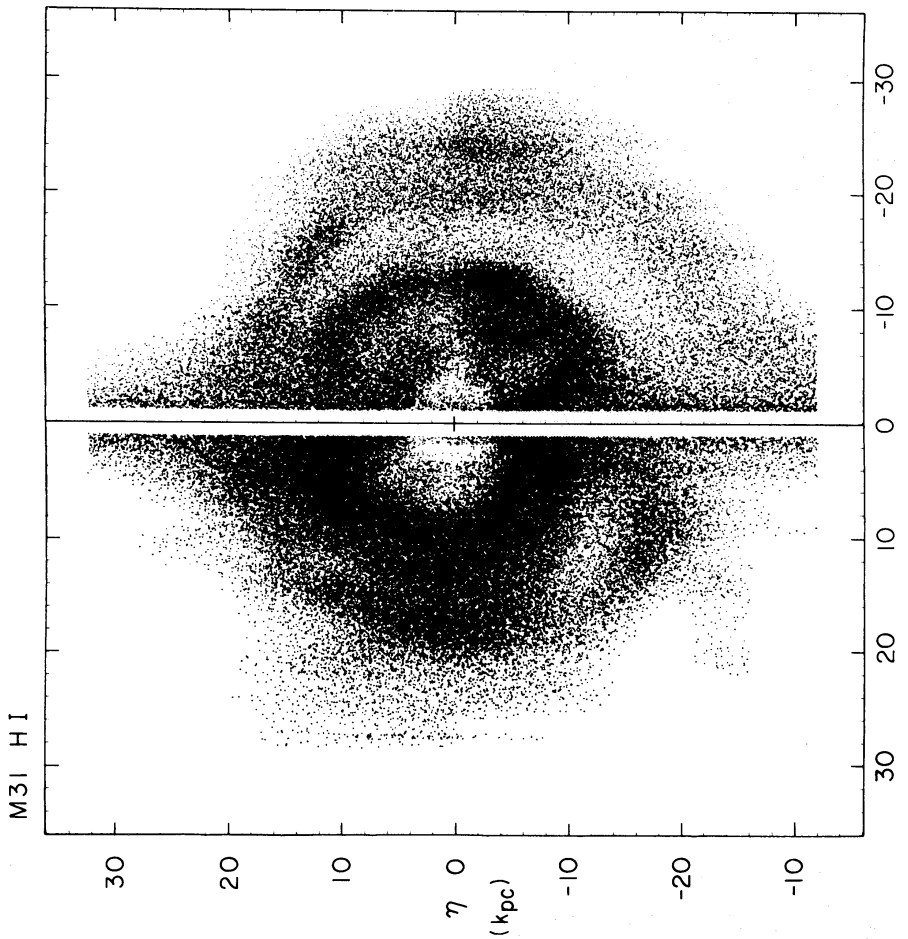

Fig. 5a. The same as figure 5c but displayed in gray scale.

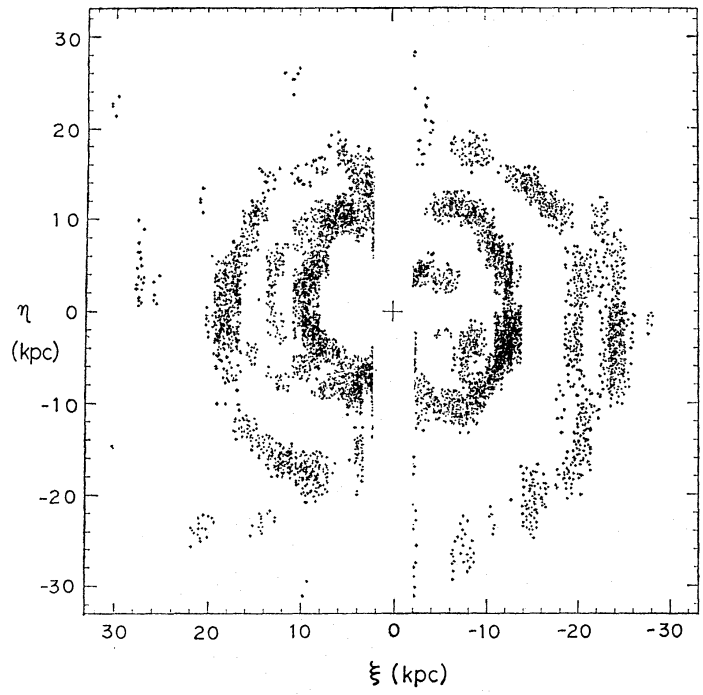

Fig. 6. Distribution of the H I ridges in M 31. This figure has been obtained by subtracting a smoothed distribution in figure 5 from the original one. [See Sofue and Reich (1979) for details.]

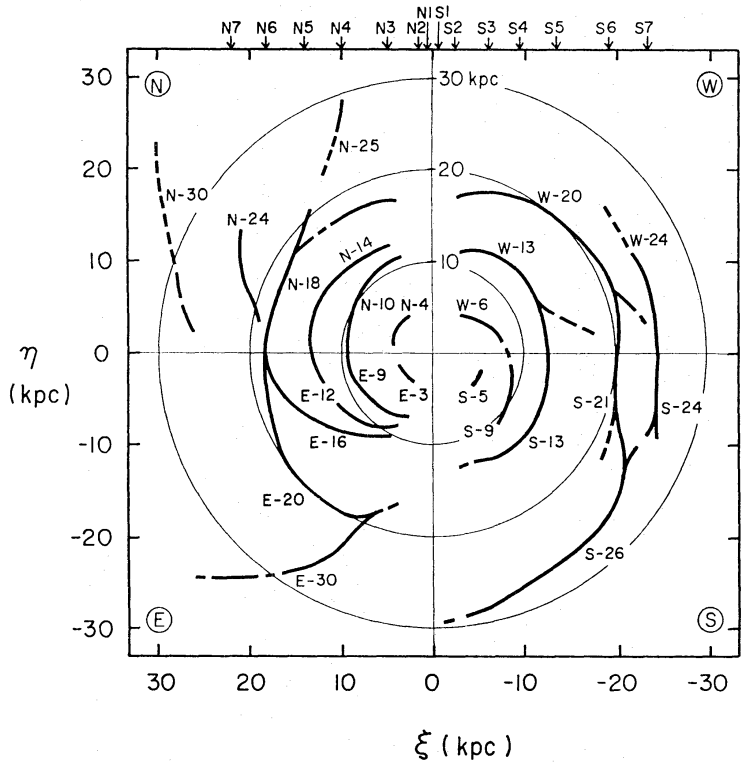

Fig. 7. Ridges of H I distribution found in figures 5 and 6. The H I ridges are labelled with such a name as "N-18" which indicates an H I ridge in the northern quadrant at a typical radial distance of $R=18$ kpc from the center. Tangential positions of Baade's (1958) arms are marked with the arrows.

(b) Dense arms in the H I ring: The H I ring consists of a few arms. The gas concentration in the arms is not uniform but patchy. Principal arms are traced by lines N-10/E-9, S-13/W-13, and N-14/E-12 (figure 7).

(c) Giant H I patch: A dense condensation of the gas is found centered at $(\xi, \eta)=(-12\,\mathrm{kpc}, -5\,\mathrm{kpc})$ with a size of 2×5 kpc on the arm S-13. The highest H I column density is $N_{\mathrm{H\,I}}\cong8\times10^{20}\,\mathrm{cm}^{-2}$ or $n_{\mathrm{H\,I}}\cong2.7\,\mathrm{cm}^{-3}$ for a disk thickness of 100 pc.

(d) SW outer arm: It is striking that a well-developed, *trailing* spiral arm, starting at $(\xi, \eta)=(-3\,\mathrm{kpc}, 18\,\mathrm{kpc})$, runs through (22 kpc, 0 kpc) and reaches (−5 kpc, −27 kpc): W-20/S-21, S-26. A bridge at $(\xi, \eta)=(-17\,\mathrm{kpc}, 4\,\mathrm{kpc})$ connects the arm and the H I ring. A sub-arm extends from (−25 kpc, 0 kpc) to (−23 kpc, 11 kpc): W-24/S-24.

(e) NE outer arms: An arm is traced from $(\xi, \eta)=(5\,\mathrm{kpc}, -16\,\mathrm{kpc})$, running through (18 kpc, 0 kpc), till (14 kpc, 20 kpc), possibly extending to (12 kpc, 30 kpc): E-20/N-18/N-25.

(f) Faint outer arms: Several outer spiral arms (spur-like features) are found;

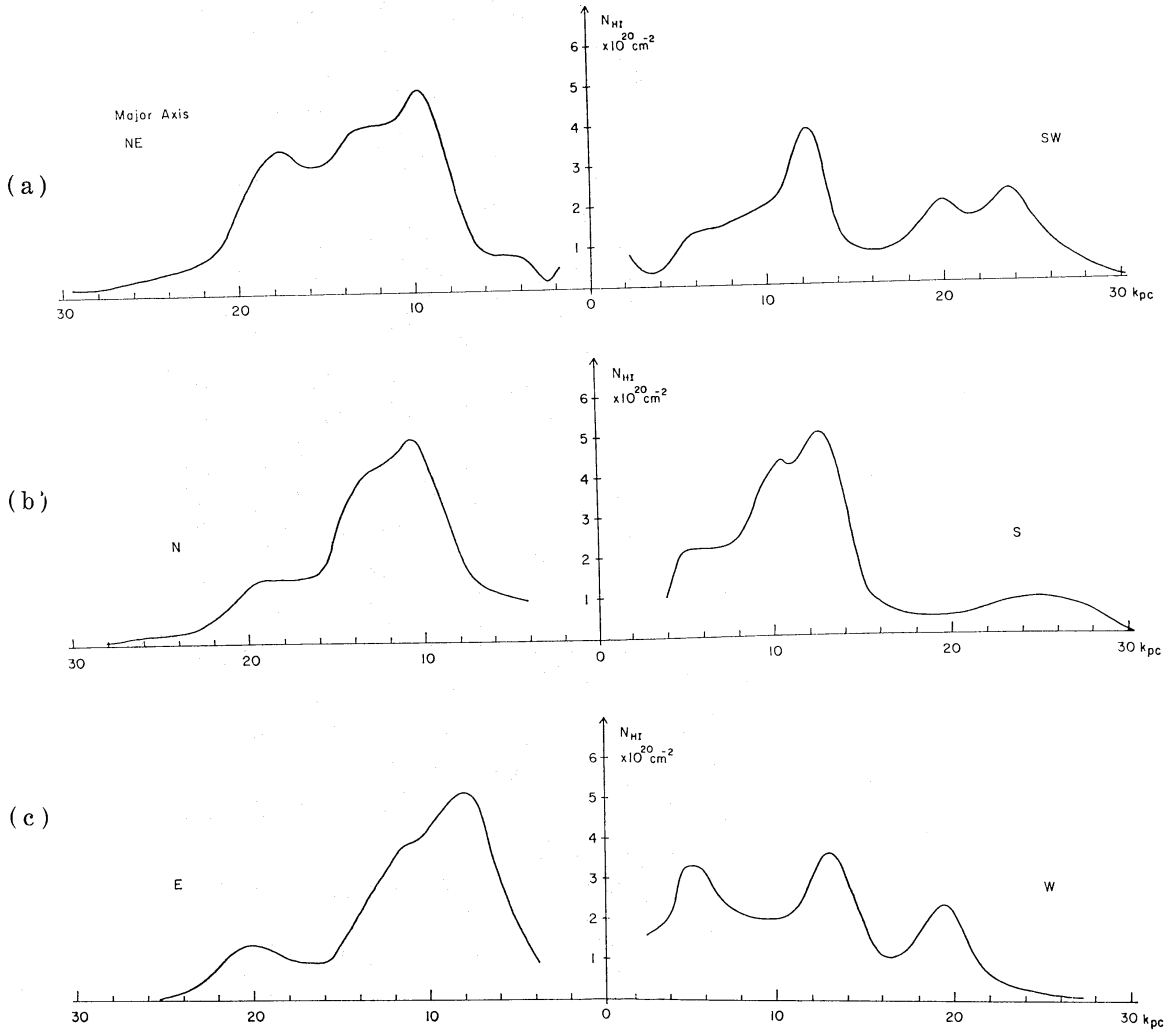

Fig. 8. Radial distributions of $N_{\mathrm{H\,I}}$ across M 31; (a) along the major axis, (b) along the NS line at 45° to the ξ-axis, and (c) along the EW line at 45° to the ξ-axis.

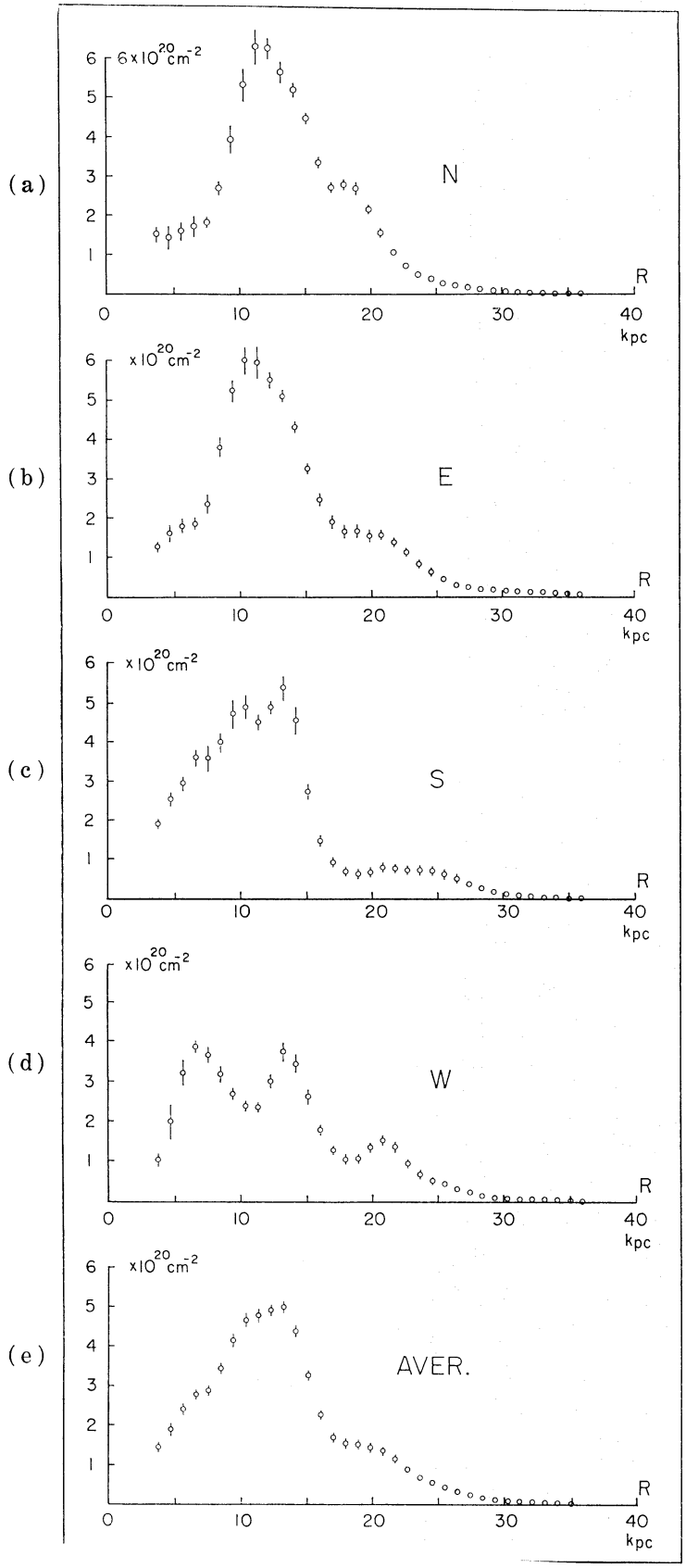

Fig. 9. Radial distributions of $N_{\mathrm{H\,I}}$ averaged over each of the four sectors divided by the ξ and η axes; (a) northern quadrant; (b) eastern quadrant; (c) southern quadrant; (d) western quadrant; and (e) all around the galaxy.

one starting from $(\xi, \eta)=(10\,\mathrm{kpc}, -20\,\mathrm{kpc})$ and reaching to (25 kpc, −25 kpc): E-30; one from (20 kpc, 8 kpc) to (22 kpc, 14 kpc): (N-24); and one from (15 kpc, 15 kpc) to (12 kpc, 30 kpc): N-25. Such faint outer arms are not found in the SW half. The outer part in the NE half of M 31 at $R \geqq 20$ kpc is more "disturbed" than in the SW half.

(g) H I edge of M 31 and asymmetry: The outer edge of the H I disk as traced by the contour level at $N_{\mathrm{H\,I}}=10^{19}\,\mathrm{cm}^{-2}$ is predominantly circular with a radius of $R=30$ kpc. However, there exists a slight elongation towards the north by 3–5 kpc. This is mainly due to the feature N-30.

(h) "H I hole:" The central region of $R \lesssim 6$ kpc lacks the H I gas, forming a "hole" with $N_{\mathrm{H\,I}}$ as low as $2\times10^{19}\,\mathrm{cm}^{-2}$ or below.

(2) Radial distribution and H I mass: We divide the galaxy into rings each 1 kpc wide, and average the column density in each ring yielding a mean column density in the ring. Figure 8 shows cross cuts across the galaxy along the major axis and along lines at ±45° to the ξ axis. Figures 9a–d show the radial distributions of the mean $N_{\mathrm{H\,I}}$ separately for the four sections in the north ($\xi>0, \eta>0$), east ($\xi>0, \eta<0$), south ($\xi<0, \eta<0$) and west ($\xi<0, \eta>0$). Figure 9e shows the same but averaged all around the individual rings.

The radial distributions show a high concentration of the H I gas in the "H I ring." The peak column density of the ring is $N_{\mathrm{H\,I}}>6\times10^{20}\,\mathrm{cm}^{-2}$. The ring has a sharp edge radially outwards. The width of the ring is not uniform, but the SW half is wider than the NE half by 20 percent. The H I mass involved by the H I ring, or the H I mass enclosed by two circles $R=8$ and 16 kpc, shares 54 percent of the total H I mass of M 31. The ring is surrounded by a broad palteau of $N_{\mathrm{H\,I}}\approx10^{20}\,\mathrm{cm}^{-2}$ extending from $R=16$ kpc to $R=30$ kpc. The plateau is slightly elongated in the direction of north-south.

(3) Spiral arms: Figures 5 and 6 show many arms traced as ridges of the H I density, which are summarized in figure 7. The most remarkable is the far outer *trailing* spiral arm, W-20/S-26. It is not easy to find a grand design of

Table 2. Correspondence between the H I arms and Baade's (1958) arms.*

Baade's (1958) arm	H I arms	Distance of the tangential position from the center
N1	—	1 kpc
N2	—	1.8
N3	N-4/E-3†	4
N4	N-10/E-9	9
N5	N-14/E-12	13
N6	N-18/E-20	18
N7	N-24	22
S1	—	0.5
S2	—	2
S3	S-5	6
S4	S-9/W-6	8
S5	S-13/W-13	13
S6	S-21/W-20	20
S7	S-24/W-24	24

* See also figure 7.

† The designation "E-3" implies an arm in the eastern quadrant at a typical radial distance of 3 kpc from the center.

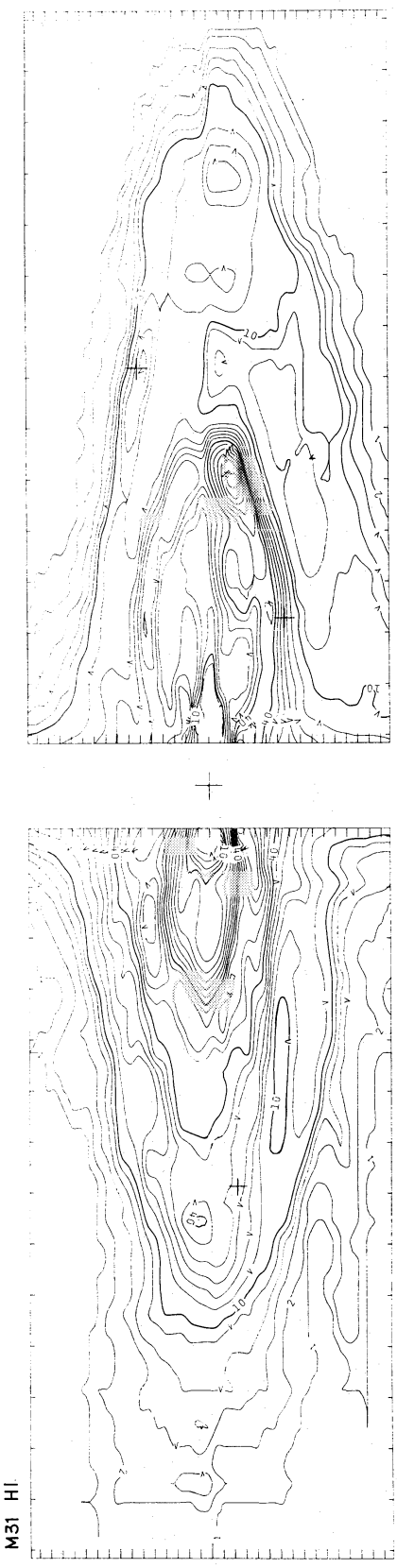

Fig. 10. Projection of the contour map of $N_{\mathrm{H\,I}}$ in figure 5 onto the plane of the sky for an inclination angle of $i=77°$. The contour units are in 10^{19} cm^{-2}.

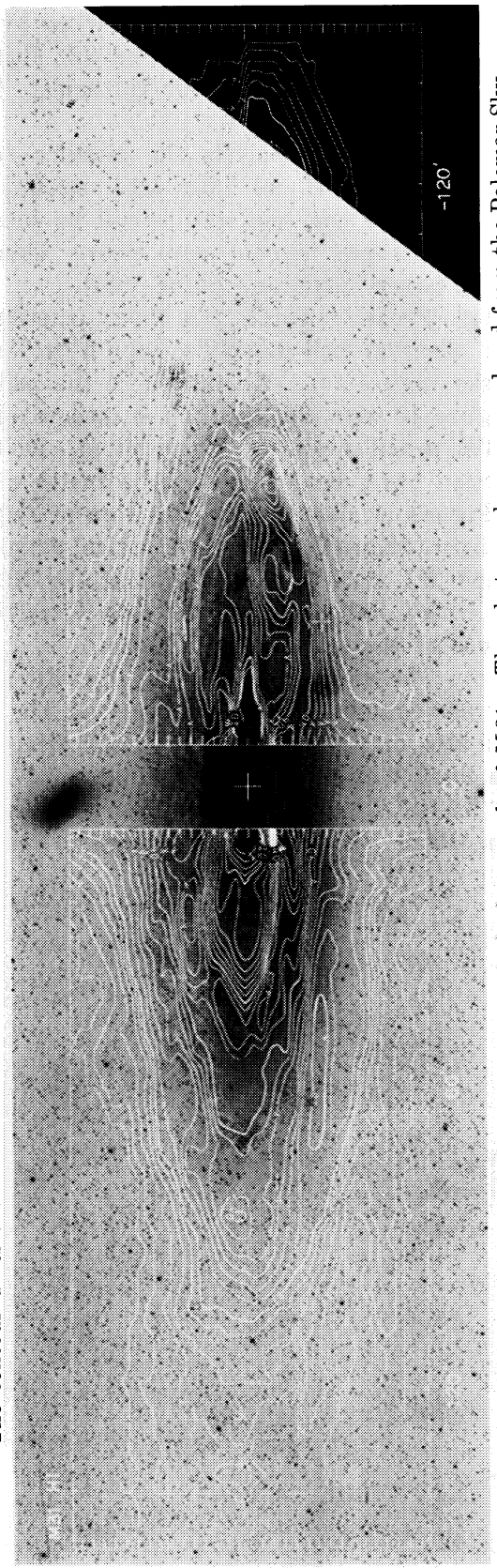

Fig. 11. Superposition of figure 10 on an optical photograph of M 31. The photograph was reproduced from the Palomar Sky Survey prints (blue).

two-armed spirals from the figures. The tangential positions of the optical arms determined by Baade (1958) are marked by arrows in figure 7. Except for the very inner arms (N1, N2, S1, and S2), Baade's (1958) arm positions coincide with the tangential positions of our H I arms. Their correspondence is summarized in table 2.

In the present analysis the circular rotation was assumed over the entire disk. However, if we take into account the density waves and non-circular motion of the gas, the results will be somewhat improved and the identification of the arms may become more clear. This problem will be discussed in a forthcoming paper (Sawa and Sofue 1981).

(*4*) *Projection onto the sky*: In order to compare our results directly with other observational data, we make a projected map of figure 5 onto the plane of the sky (figure 10). We take here the inclination angle of $i=77°$. A comparison of figure 10 with the map of the integrated H I gas distribution obtained by the 9′ HPBW pencil beam by Cram et al. (1980) reveals that the resolution in the η-direction has been improved by a factor of ~ 4.

Figure 11 shows a superposition of the contour map on an optical photograph. The figure shows that the main optical arms at radii $R=8$–15 kpc are accompanied by the H I arms, which are near the "H I ring." In the inner region at $R<8$ kpc, where optical arms are better traced, the coincidences are not so clear because of the lack of the H I gas.

(*5*) *The arms traced on* $T_A(\lambda, v)$ *diagram*: We have so far obtained the arms as positions of enhanced N_{HI} on the (ξ, η) coordinates. We can trace the arms also on the $T_A(\lambda, v)$ diagrams directly obtained from the velocity profiles. At a fixed β and λ, the antenna beam covers effectively an area of $\delta\xi \times \delta\eta = 1.8$ kpc $\times$ 8.5 kpc. In figure 12 we reproduce a $T_A(\lambda, v)$ diagram at $\beta=-18'$ from Cram et al. (1980). We find some bifurcated features as traced on the figure by the

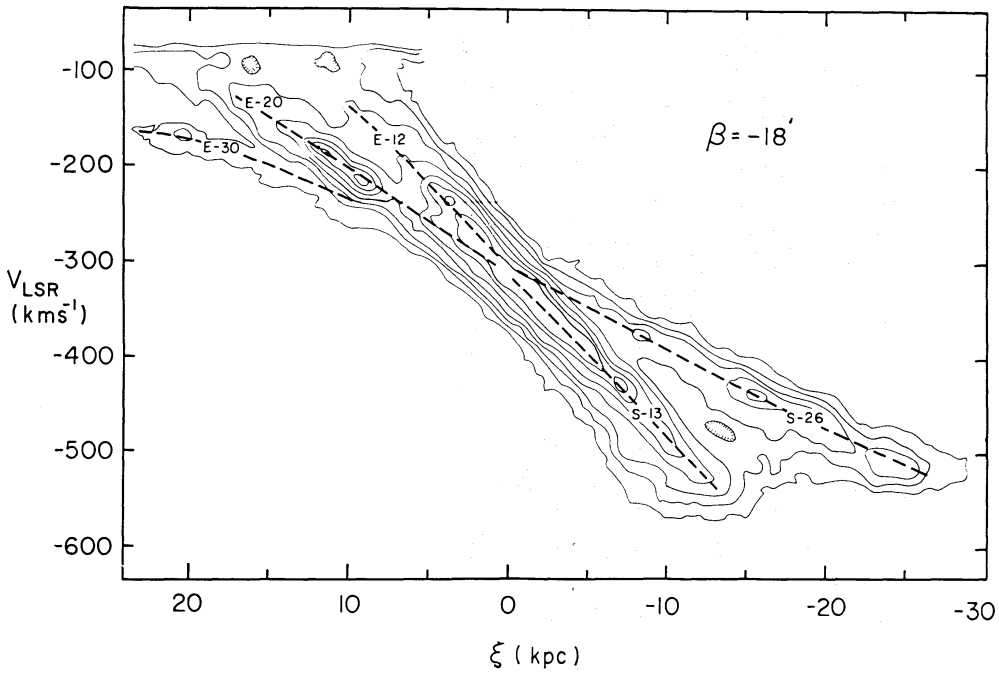

Fig. 12. The $T_A(\lambda, v)$ diagram at $\beta=-18'$ reproduced from Cram et al. (1980). The dashed lines correspond to the H I arms in figure 7 with the same labels.

lines E-12, E-20, E-30, S-13 and S-26. The ridges correspond to the arms with the same names in figure 7. Such bifurcations in $T_A(\lambda, v)$ diagram are well known in our galaxy representing the positions of the spiral arms (Weaver 1974; Burton 1976). The bifurcated features in M 31 have been noted by Cram et al. (1980) and by Henderson (1979), who consider the bifurcation as due to a warping of the galaxy disk. Byrd (1978) has interpreted it as due to a tidal disturbance by the companion galaxy M 32.

5. Discussion

The H I gas distribution in M 31 is characterized by the "H I ring" of width $\sim$6 kpc, centered at the radius R=12 kpc. The ring-like structure may be common to spiral galaxies as has been demonstrated for our Galaxy (e.g. Burton 1976) and M 81 (Rots and Shane 1975). However, the degree of the gas concentration in the ring of M 31 is much higher than in other galaxies and the outer edge of the ring is more steeply defined. The origin and formation of such a large-scale and high-contrast ring of gas remains open to question.

The H I ring consists of a few arms and patches. Among them the giant H I patch at $(\xi, \eta)=(-12\,\text{kpc}, -5\,\text{kpc})$ is remarkable. Arp (1964) suggested a connection of M 32 to an optical spiral arm which coincides with the H I arm, S-13, associated with this giant patch. We only suggest here that a tidal disturbance by M 32 would have produced such a high condensation of gas, when it crossed the plane of M 31. Byrd (1978) has simulated the tidal interaction between the M 31 disk and M 32.

The H I ring is surrounded by a plateau of low-surface density up to the radius $R\sim$30 kpc. Many outer arms are superimposed on the plateau. A part of the SW outer arm (S-21, S-24/W-24) has been noticed by some authors as the SW neutral hydrogen companion (e.g. Emerson 1974). The outer edge of M 31 as seen by H I gas is slightly asymmetric and elongated to the north, where is found a faint spur-like spiral arm, N-30. The asymmetry could have been caused by tidal interaction with the larger companion NGC 205, or with another more distant but massive galaxy like M 33.

The VST method proposed in this paper can be applied not only to highly-tilted galaxies like M 31 but also to edge-on galaxies for deriving their spiral arms, provided we have a mean to distinguish the far side from the near side on the line of sight for a certain radial velocity. This could be done, for example, by assuming some appropriate shape of the arms like bisymmetric and trailing logarithmic spirals. For mildy tilted galaxies the VST provides a mean to improve the spatial resolution in the direction of the minor axis.

The authors thank Professor M. Fujimoto for his discussion and encouragement. They are indebted to Drs. M.S. Roberts and T.R. Cram for making their H I line data avialable in the form of a magnetic tape. They are also indebted to Professor R.N. Whitehurst for valuable comments and useful suggestions. This work was supported in part by the Scientific Research Fund of Ministry of Education, Science, and Culture under Grant No. 542003 (Y. Sofue in FY 1980 and 1981).

References

Arp, H. 1964, *Astrophys. J.*, **139**, 1045.
Baade, W. 1958, *Ric. Astron. Specola Vaticana*, **5**, 1.
Baade, W., and Arp, H. 1964, *Astrophys. J.*, **139**, 1027.
Beck, R. 1979, Ph. D. Thesis, Bonn University.
Beck, R., Berkhuijsen, E.M., and Wielebinski, R. 1980, *Nature*, **283**, 272.
Berkhuijsen, E.M. 1977, *Astron. Astrophys.*, **57**, 9.
Blitz, L., Fich, M., and Stark, A.A. 1979, in *Interstellar Molecules, IAU Symposium No. 87*, ed. B. H. Andrew (Reidel, Dordrecht), p. 213.
Burton, W.B. 1976, *Ann. Rev. Astron. Astrophys.*, **14**, 275.
Byrd, G.G. 1978, *Astrophys. J.*, **226**, 70.
Cram, T.R., Roberts, M.S., and Whitehurst, R.N. 1980, *Astron. Astrophys. Suppl.*, **40**, 215.
Davies, R.D., and Gottesman, S.T. 1970, *Monthly Notices Roy. Astron. Soc.*, **149**, 237.
Emerson, D.T. 1974, *Monthly Notices Roy. Astron. Soc.*, **169**, 607.
Emerson, D.T. 1976, *Monthly Notices Roy. Astron. Soc.*, **176**, 321.
Gottesman, S.T., and Davies, R.D. 1970, *Monthly Notices Roy. Astron. Soc.*, **149**, 263.
Guibert, J. 1973, *Astron. Astrophys. Suppl.*, **12**, 263.
Guibert, J. 1974, *Astron. Astrophys.*, **30**, 353.
Henderson, A.P. 1979, *Astron. Astrophys.*, **75**, 311.
Kerr, F.J., and Westerhout, G. 1965, in *Galactic Structure*, ed. A. Blaauw and M. Schmidt (University of Chicago Press, Chicago), p. 167.
Kormendy, J., and Norman, C.A. 1979, *Astrophys. J.*, **233**, 539.
Pellet, A., Astier, N., Viale, A., Courtès, G., Maucherat, A., Monnet, G., and Simien, F. 1978, *Astron. Astrophys. Suppl.*, **31**, 439.
Pooley, G.G. 1969, *Monthly Notices Roy. Astron. Soc.*, **144**, 101.
Reich, W., Kalberla, P., and Neidhöfer, J. 1976, *Astron. Astrophys.*, **52**, 151.
Richter, G.A. 1971, *Astron. Nachr.*, **292**, 275.
Roberts, M.S. 1966, *Astrophys. J.*, **144**, 639.
Roberts, M.S., and Whitehurst, R.N. 1975, *Astrophys. J.*, **201**, 327.
Rots, A.H., and Shane, W.W. 1975, *Astron. Astrophys.*, **45**, 25.
Rubin, V.C., and Ford, W.K., Jr. 1970, *Astrophys. J.*, **159**, 379.
Sawa, T., and Sofue, Y. 1981, *Publ. Astron. Soc. Japan*, **33**, No. 4, in press.
Shane, W.W. 1975, in *"La dynamique des galaxies spirals,"* ed. L. Weliachew (Centre National de la Recherche Scientifique, Paris), p. 257.
Simien, F., Athanassoula, E., Pellet, A., Monnet, G., Maucherat, A., and Courtès, G. 1978, *Astron. Astrophys.*, **67**, 73.
Sofue, Y., and Reich, W. 1979, *Astron. Astrophys. Suppl.*, **38**, 251.
Unwin, S.C. 1980a, *Monthly Notices Roy. Astron. Soc.*, **190**, 551.
Unwin, S.C. 1980b, *Monthly Notices Roy. Astron. Soc.*, **192**, 243.
van den Bergh, S. 1964, *Astrophys. J. Suppl.*, **9**, 65.
Weaber, H., 1974, in *Galactic Radio Astronomy, IAU Symposium, No. 60*, ed. F.J. Kerr and S.C. Simonson, III (Reidel, Dordrecht), p. 573.
Whitehurst, R.N., and Roberts, M.S. 1972, *Astrophys. J.*, **175**, 347.
Whitehurst, R.N., Roberts, M.S., and Cram, T.R. 1978 in *Structure and Properties of Nearby Galaxies, IAU Symposium No. 77*, ed. E.M. Berkhuijsen and R. Wielebinski (Reidel, Dordrecht), p. 175.